Chem Rev Lett 9 (2026) 209-222

Research Article

Chemical Review and Letters
journal homepage: www.chemrevlett.com
ISSN (online): 2645-4947 (print) 2676-7279

A computational insight into the structural analysis and electronic properties of altretamine anticancer drug complexed with group IIA (Mg^{2+}, Ca^{2+}) metal ions, quasi-metal (Si^{2+}, Ge^{2+}) ions, and transition metal (Fe^{2+}, Zn^{2+}) ions

Fahimeh Alirezapour[1,*], Kourosh Bamdad[1], Marjan Jokar[1], Azadeh Khanmohammadi[1]

[1]*Department of Chemistry, Payame Noor University (PNU), P.O. Box 19395-4697, Tehran, Iran.*

ARTICLE INFO

Article history:
Received 24 November 2025
Received in revised form 25 December 2025
Accepted 25 January 2026

Keywords:
Altretamine
DFT
AIM
NBO
NMR
Aromaticity indices

ABSTRACT

In the present study, density functional theory (DFT/ωB97XD) is employed to investigate cation–π interactions in Altretamine–M (M = Fe^{2+}, Zn^{2+}, Si^{2+}, Ge^{2+}, Mg^{2+}, and Ca^{2+}) complexes in both the gas phase and solution. Overall, metals contribute to drug interactions through coordination chemistry, redox activity, enzyme modulation, metabolic transformations, and effects on pharmacokinetics and pharmacodynamics. Metals, either as components of a drug or through interactions with metal ions, can also influence drug solubility, stability, and delivery, thereby affecting absorption and bioavailability. The results show that the binding strength in the gas phase is higher than in the solution. The chemical bonding properties and population analysis of the structures are evaluated using the atoms-in-molecules (AIM) and natural bond orbital (NBO) analyses. According to the results, cation-π interactions in the complexes are of a closed-shell nature. The aromaticity of the complexes is assessed using two widely recognized indices, which facilitate detailed evaluation of the electronic structure and aromatic character of the molecules. The NMR analysis is performed to calculate some coupling constants and nitrogen shielding tensors in the complexes. Finally, the electronic properties of structures are estimated using conceptual DFT parameters.

1. Introduction

Altretamine (ALT) is an anticancer drug mostly used for the palliative treatment of persistent or recurrent ovarian cancer, particularly after initial treatment with cisplatin or combinations of alkylating agents [1]. It is a small-molecule drug that acts as an alkylating agent. ALT breaks down through N-demethylation into alkylating agents that harm tumor cells by interfering with DNA and RNA production [2]. This drug is highly soluble in lipids and is also known as hexamethylmelamine (HMM) [3]. While ALT has relatively low liver toxicity, it can temporarily lower white blood cells and platelets, which raises the risks of infections and bleeding [4]. ALT is primarily used for ovarian cancer, but it may also be considered for second-line treatment in other cancers [5].

The interaction between drugs and cations through cation-π interactions involves the attraction between a positively charged cation, often a metal ion or a group on the drug, and the negatively charged electron cloud of an aromatic ring within the drug molecule or receptor [6-13]. The interaction energy depends on the type of cation and the π system, which plays a key role in molecular recognition [14]. In drug-receptor binding, cation-π interactions play a crucial role in stabilizing the drug in aromatic-rich binding sites, thereby enhancing specificity and affinity [15-20]. These interactions also contribute to binding in various biological systems, such as acetylcholine receptors, neurotransmitter binding, and enzyme active sites [21-26]. In silico modeling and structural studies demonstrate how cation-π interactions are involved in drug binding, guiding the design of drugs to enhance potency and selectivity [27-35]. Thus, cation-π interactions are a vital non-covalent binding force in pharmaceuticals. Cations interact with aromatic π systems to stabilize drug-target complexes and affect pharmacodynamics [36-45].

Metals can significantly affect drug solubility, stability, and delivery using their interactions with metal ions. This influences absorption and bioavailability in several ways. For instance, Metal ions can form coordination complexes with drug molecules. This

* Corresponding author E-mail: falirezapoor@pnu.ac.ir
https://doi.org/10.22034/crl.2026.561943.1740

changes the solubility of the drug by increasing its ability to dissolve in water or fat, depending on the metal and ligand involved. Such complexation often improves aqueous solubility, which is crucial for bioavailability in oral administration [46-48]. Coordination bonds between metals and drugs enhance molecular stability. This prevents degradation or aggregation during manufacturing and storage. The improved stability extends shelf-life and boosts therapeutic effectiveness [49-51]. Metal-drug complexes can change drug release profiles and delivery in the body. They enable sustained or targeted release, as seen in metal-coordinated nanoparticles and hydrogels used in drug delivery systems [52]. Additionally, drug-metal complexation can affect pharmacokinetics by changing distribution coefficients and membrane permeability. This ultimately influences overall bioavailability [53]. Using metal coordination thoughtfully can improve drug formulation, as seen in metallodrugs and drug delivery systems designed for better solubility, stability, and targeted therapeutic effects [54, 55].

The characteristics and energies of cation-π interactions have been the focus of numerous studies [56–61]. In 2019, Mohammadi et al. [62] applied the DFT method to analyze complexes formed between the acetaminophen drug with alkali-metal and alkaline-earth cations. Additional studies by Alirezapour et al. [63] examined the structural and electronic effects of metal cations interacting with the π-system of phenylalaninal in various environments, which helps elucidate how these cations influence molecular stability and behavior. In 2020, a similar computational investigation was conducted to explore cation-π interactions between the anticancer drug altretamine and metal cations, evaluating the stability and electronic properties of these drug-metal complexes [64]. Lastly, the effect of cation-π interactions on the structural and electronic features of para-aminosalicylic acid complex was assessed in 2020 [65].

Our objective is to explore the energetic, geometric, spectroscopic, and topological properties of Altretamine anticancer drug complexed with transition metal ions, quasi-metal ions, and group IIA metal ions. To these evaluations, we apply the DFT method, along with the AIM and NBO analyses. To determine the aromaticity and electron delocalization in complexes, different aromaticity indices are considered. Finally, the electronic properties of complexes are estimated using conceptual DFT parameters. These investigations provide vital insights into the nature of cation-π interactions, showing that cations can form stable complexes with drugs through interactions with aromatic or π-electron systems, which alter drug properties such as stability and reactivity [66-70].

This study stands out by including quasi-metal ions like Si^{2+} and Ge^{2+} alongside conventional group IIA (Mg^{2+}, Ca^{2+}) and transition metals (Fe^{2+}, Zn^{2+}), which are rarely combined in single investigations of Altretamine complexes. Employing computational tools for structural optimization, vibrational analysis, and electronic properties provides fresh atomic-level insights absent in experimental-only studies of similar chelates. This approach highlights potential stability enhancements or reactivity shifts for pharmaceutical applications, differentiating it from heterocyclic metal complexes focused on synthesis rather than predictive modeling. No prior publications directly simulate Altretamine with Si^{2+}/Ge^{2+} or juxtapose them against Mg^{2+}/Ca^{2+} and Fe^{2+}/Zn^{2+}, filling a void in understanding metal-induced modifications to Altretamine's aromaticity and bioactivity.

2. Quantum chemical calculations

The Gaussian 09 suite of programs [71] is used to perform all calculations on monomers and complexes. The method and basis set used to optimize the structures are ωB97XD [72] and 6-311++G(d,p) [73], respectively. The ωB97X-D functional is a long-range corrected hybrid DFT method designed for accurate treatment of thermochemistry, kinetics, and non-covalent interactions [74]. It builds on the ωB97X functional by incorporating empirical atom-atom dispersion corrections with a damped function, addressing limitations in van der Waals interactions. The range-separation parameter ω = 0.2 $bohr^{-1}$ splits short-range DFT exchange from long-range Hartree-Fock exchange, improving charge-transfer and dispersion descriptions [75]. Geometry optimizations require explicit reporting of convergence criteria to ensure reproducibility. Force convergence typically targets a maximum gradient below 3×10^{-4} hartree/bohr, while RMS force is set under 1×10^{-4} hartree/bohr. Displacement convergence often uses an RMS step below 2×10^{-3} bohr and a maximum displacement under 4×10^{-3} bohr [76]. In the Gaussian, "opt = tight" enforces an RMS force of 3×10^{-4} and a maximum force of 4.5×10^{-4} hartree/bohr. SCF convergence also includes tighter settings like TightSCF, which reduce gradient noise [77].

One of the most important calculations on the optimized structures is the evaluation of vibrational frequencies. These results are obtained at the same theoretical level. The binding energy ($\Delta E_{ion-\pi}$) of the ALT monomer and the metal cations is calculated as follows:

$$\Delta Eion\text{-}\pi = Ecation\text{-}\pi - (Ecation + E\pi\text{-}system) \quad (1)$$

where the total energy of the complexes, the energy of the ALT monomer, and the energy of the isolated cations are shown as $E_{cation-\pi}$, $E_{\pi-system}$, and E_{cation}, respectively. Boys and Bernardi's counterpoise method is applied to correct basis set superposition error (BSSE) [78]. The effect of the solvent on the complexes is evaluated using the self-consistent reaction field (SCRF) method combined with the polarized continuum model (PCM) [79].

The chemical bonding properties and population analysis of the structures are evaluated using the AIM [80] and NBO [81] analyses. The AIM 2000 package [82] is used for the AIM analysis. These calculations are performed on optimized structures at the ωB97XD/6-311++G(d,p) level. The highest occupied molecular orbital (HOMO) and the lowest unoccupied molecular orbital (LUMO), known as frontier molecular orbitals (FMOs), evaluate the electronic properties of the selected complexes. The aromaticity of the ALT ring is examined using two well-known indices of the harmonic oscillator model of aromaticity (HOMA) [83] and the aromatic fluctuation index (FLU) [84]. The results are obtained with the Multiwfn 3.7 program [85]. Finally, NMR analysis is performed to calculate some coupling constants and nitrogen shielding tensor in the selected complexes [86].

3. Results and Discussion

3.1. Energies

A schematic of the optimized ALT···M complexes with M = Fe^{2+}, Zn^{2+}, Si^{2+}, Ge^{2+}, Mg^{2+}, and Ca^{2+} is shown in Fig. 1. Table 1 lists the binding energies ($\Delta E_{ion-\pi}$) of the cations and the selected π system. The trend in $\Delta E_{ion-\pi}$ values of the complexes is as follows: $Fe^{2+} > Si^{2+} > Zn^{2+} > Ge^{2+} > Mg^{2+} > Ca^{2+}$. The results obtained show that the strength of the cation-π interaction in complexes containing Fe^{2+} and Si^{2+} ions is the highest, while the lowest values are observed in complexes containing Mg^{2+} and Ca^{2+} ions. According to the results in Table 1, the solvent effect leads to significant changes in the binding energy results. The data show that the strength of cation-π interaction in the gas phase is greater than in solution. In the solution phase, the quasi-metal complexes (Si^{2+} and Ge^{2+}) exhibit stronger interactions than the other metal complexes. The binding energy of the Si^{2+} complex in the gas phase is -227.28 kcal/mol, which decreases significantly to -91.79 kcal/mol in the aqueous solvent (Table 1).

Under standard conditions of one atmosphere pressure and 298.15 Kelvin, thermodynamic parameters such as entropy (ΔS), enthalpy (ΔH), and Gibbs free energy (ΔG) are calculated to gain better insight into the properties of the considered complexes. The data obtained are summarized in Table 1. As shown in this table, the calculated ΔH values are negative. This indicates that the formation of all complexes is enthalpically favorable (exothermic). On the other hand, the ΔG values are positive. This means that the formation of the complexes is a non-spontaneous process. The obtained ΔS values are also negative and $|\Delta H| < |T\Delta S|$. This implies that the entropy factor controls the stability of the complexes. Therefore, it can be concluded that the nature of the different cations plays an important role in the values of the thermodynamic parameters.

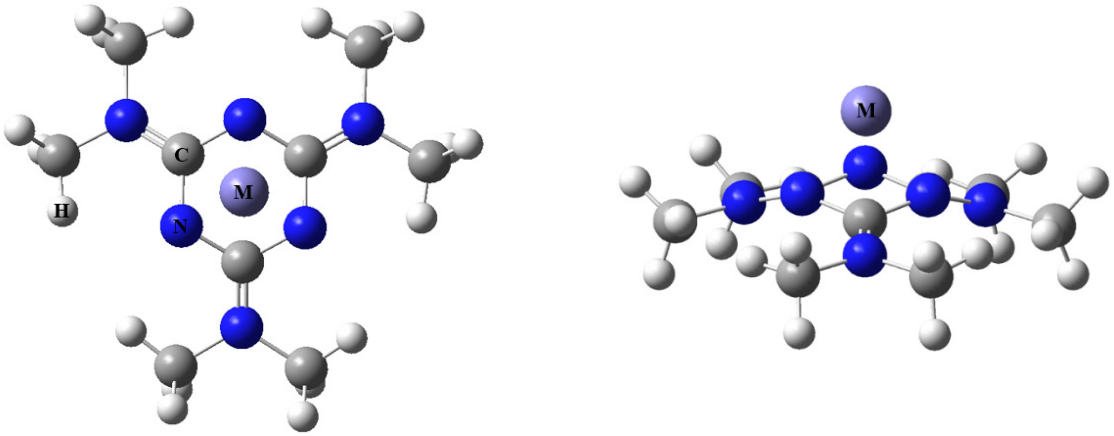

(a) (b)

Fig. 1. The model representation for the ALT···M complexes, with M = Fe^{2+}, Zn^{2+}, Si^{2+}, Ge^{2+}, Mg^{2+}, and Ca^{2+} from front view (a) and top view (b).

Table 1. Binding energy values ($\Delta E_{ion-\pi}$, in kcal/mol), geometrical parameters (bond length (d), **i**n Å), stretching frequencies (υ, in cm^{-1}) of ion-π, and thermodynamic parameters of complex formation (ΔH, ΔG and ΔS, in kcal/mol).

	$\Delta E_{ion-\pi}$	$d_{ion-\pi}$	$\upsilon_{ion-\pi}$	ΔH_{298}	ΔG_{298}	ΔS_{298}
Fe^{2+}	-258.79 (-18.95)[a]	1.603	463.89	-0.683	8.565	-0.031
Zn^{2+}	-205.02 (-19.30)	1.797	291.00	-0.845	8.628	-0.032
Si^{2+}	-227.28 (-91.79)	1.739	447.76	-1.822	9.932	-0.039
Ge^{2+}	-200.52 (-68.01)	1.895	302.00	-0.398	8.313	-0.029
Mg^{2+}	-149.48 (-0.69)	1.844	393.19	-1.695	9.429	-0.037
Ca^{2+}	-113.43 (-1.02)	2.163	304.89	-0.060	6.851	-0.023

[a] Values in parentheses refer to the obtained binding energies in the water solvent.

3.2. Geometric parameters and spectroscopic data

The results of the structural parameters are reported in Table 1. The $d_{ion-\pi}$ (distance between the ion and the center of the aromatic ring) is an important quantity for assessing the strength of cation-π interactions. In the investigated complexes, there is an inverse relationship between binding energy and interaction distance ($d_{ion-\pi}$). According to the results, in each ion group, Fe^{2+}, Si^{2+}, and Mg^{2+} complexes have the highest $\Delta E_{ion-\pi}$ and the lowest $d_{ion-\pi}$. On the other hand, an inverse relationship exists between these quantities in Zn^{2+}, Ge^{2+}, and Ca^{2+} complexes.

A measurable relationship can also be observed between the geometric parameters and spectroscopic data. Table 1 lists the vibrational frequencies ($\upsilon_{ion-\pi}$) of ALT complexes. It is well known that stronger cation-π interactions shift vibrational frequencies to higher values. The data in Table 1 indicate that the relationship between $\Delta E_{ion-\pi}$ and $\upsilon_{ion-\pi}$ is consistent with the studied complexes in each ion group. Based on the calculated results, the largest shifts are in the Fe^{2+}, Si^{2+}, and Mg^{2+} complexes with higher $\Delta E_{ion-\pi}$, and the smallest shifts are in the Zn^{2+}, Ge^{2+}, and Ca^{2+} complexes with lower $\Delta E_{ion-\pi}$.

3.3. AIM analysis

The chemical properties of the atom and bonds in the structure are investigated by analyzing AIM. The quantities used in this method include electron density (ρ) and its Laplacian ($\nabla^2\rho$), as well as total electron energy density (H), along with its components containing potential energy density (V), and kinetic energy density (G) at critical bond points (BCPs). An important relationship can be observed between the Laplacian and the energy quantities at critical points [80], as shown below:

$$\frac{1}{4}\nabla^2\rho(r) = 2G(r) + V(r) \text{ and } H(r) = G(r) + V(r) \quad (2)$$

The interaction characteristics between species are measured by the Laplacian of the electron density and the sum of principal curvatures as $\nabla^2\rho = \lambda_1 + \lambda_2 + \lambda_3$. The perpendicular curvatures (λ_1 and λ_2) of electron density at the BCP are negative, while the parallel curvature (λ_3) is positive. The charge concentration is determined by the ratio $|\lambda_1|/\lambda_3$ at the bond critical points [87].

Moreover, there are two distinct benchmarks on the features of bonding, including the bond ellipticity (ε) and the Virial theorem [88]. The ellipticity of bonds (ε) affords the comparative accumulation of the two perpendicular axes and could be described as

$$\varepsilon = \lambda1/\lambda2 - 1, \text{ where } |\lambda2| < |\lambda1| \quad (3)$$

where $\lambda_1 < \lambda_2 < 0 < \lambda_3$ represent the eigenvalues of the Hessian related to the BCP electron density. The benchmark of the character of π–bond for each interaction is the ε, which provides criteria for σ and π bond characters. Lower values of ε represent the bond character of σ, whilst the greater amount of ε (> 0.1) demonstrates the bond character of π [88]. According to Table 2, the parameters of ellipticity for ion···π bonding of Si^{2+} and Ge^{2+} complexes are 0.0492 and 0.0490, respectively, and it could be considered as the bond character of σ, but the ellipticity for the ion···π bonding of other complexes is bigger than 0.1 and could be considered as π bonding.

The Laplacian of the electron charge density is locally depleted ($\nabla^2\rho_{BCP} > 0$) or concentrated ($\nabla^2\rho_{BCP} < 0$). A negative value indicates shared-shell interactions such as covalent bonds, and a positive value denotes closed-shell interactions such as ionic and van der Waals interactions. In addition, the partially covalent nature of the interactions is defined by the quantities $\nabla^2\rho_{BCP} > 0$ and $H_{BCP} < 0$. The topological parameters in Table 2 show that cation-π interactions are of a closed-shell nature. This is due to the small values of ρ_{BCP}, $\nabla^2\rho_{BCP} > 0$, and $|\lambda_1|/\lambda_3 < 1$. In complexes with transition metal ions and quasi-metal ions, because of their negative H values ($H_{BCP} < 0$), they have a partially covalent nature. On the other hand, the group IIA metal complexes exhibit a non-covalent character ($H_{BCP} > 0$).

The amounts of the charge density (ρ) at BCP have been implemented to illuminate bond strength. In other words, the notable values of ρ uncover that there exists substantial interaction between vicinal atoms. When the amount of ρ is more than 0.1 au, the presence of potent interactions, for instance, electrostatic interactions or hydrogen bonding, can be concluded. Besides, when the amount of ρ is lower than 0.1, weaker interactions such as van der Waals can be deduced. Our computed achievements divulged that the ρ_{BCP} values of the studied complexes are weak interactions. Furthermore, the results show that for each ion group, ρ_{BCP} values have a direct relationship with the binding energies. The molecular graph and contour plot of the ALT···Fe^{2+} complex are shown in Figure 2. In this Figure, three (3, -1) BCPs are formed between the metal ion and the ring nitrogen atoms in the corresponding complex. To better understand the nature of interactions, the electron localization function (ELF) of the ALT···Fe^{2+} complex is also imagined (see Figure 3).

The -G/V ratio can also assess the properties of cation-π interactions [89]. Indeed, there are three categories for interaction types, namely covalent bonding (G(r)/V(r) = 0.1–0.5), polar covalent interaction (G(r)/V(r) = 0.5–1), and electrostatic attraction (G (r)/V(r)> 1). The results obtained in Table 2 show that the -G/V ratio lies in the range 0.5496-1.0852. Based on these findings, the cation-π interactions in the Mg^{2+} and Ca^{2+} complexes are of the type electrostatic attraction, while in the other complexes, the polar covalent interaction is observed.

The reduced density gradient (RDG) method is also used to gain insight into the cation-π interactions. The Multiwfn program [85] is applied to virtualize the map.

The colored RDG diagrams show the binding nature and interaction regions in the complexes. The blue and green colors indicate strong and weak attractions, respectively, while the red color directs repulsive interactions. The iso-surface map of the RDG for the ALT···Fe^{2+} complex is depicted in Figure 4. The strength of cation-π interaction in the ALT···Fe^{2+} complex is revealed by the blue and red regions, which are created between the chosen ion and the center of the aromatic ring. Steric effects are significantly affected by red areas.

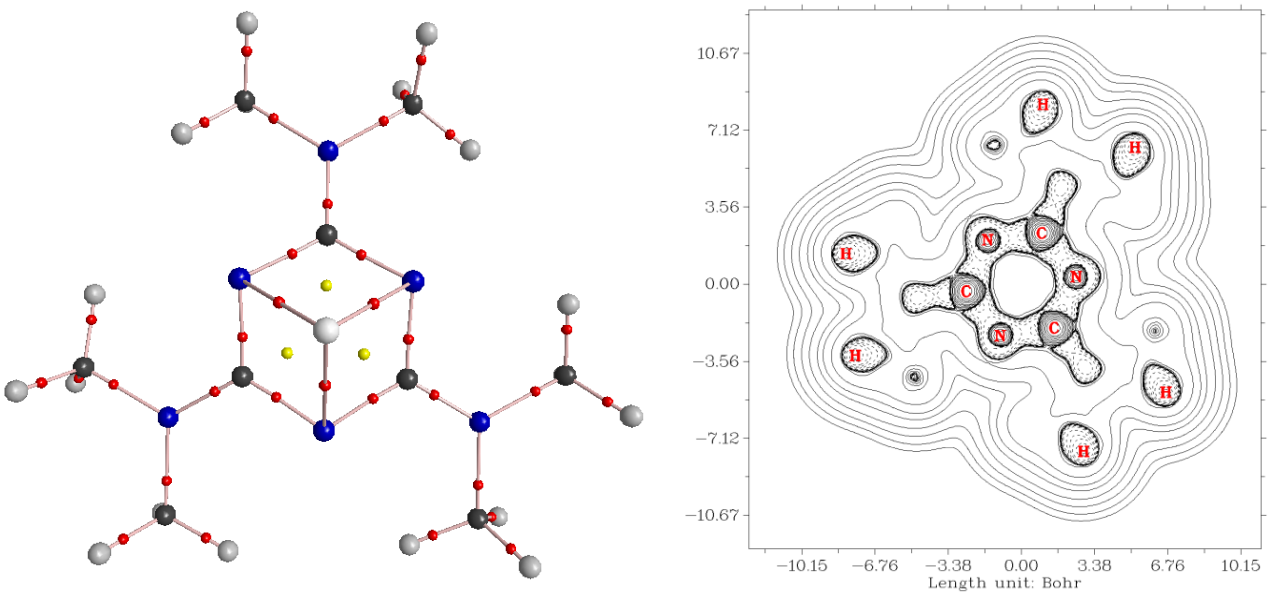

(a) (b)

Fig. 2. Molecular graph (a) and contour map (b) of ALT···Fe^{2+} complex obtained from ωB97XD/6-311++G(d,p) wave function.

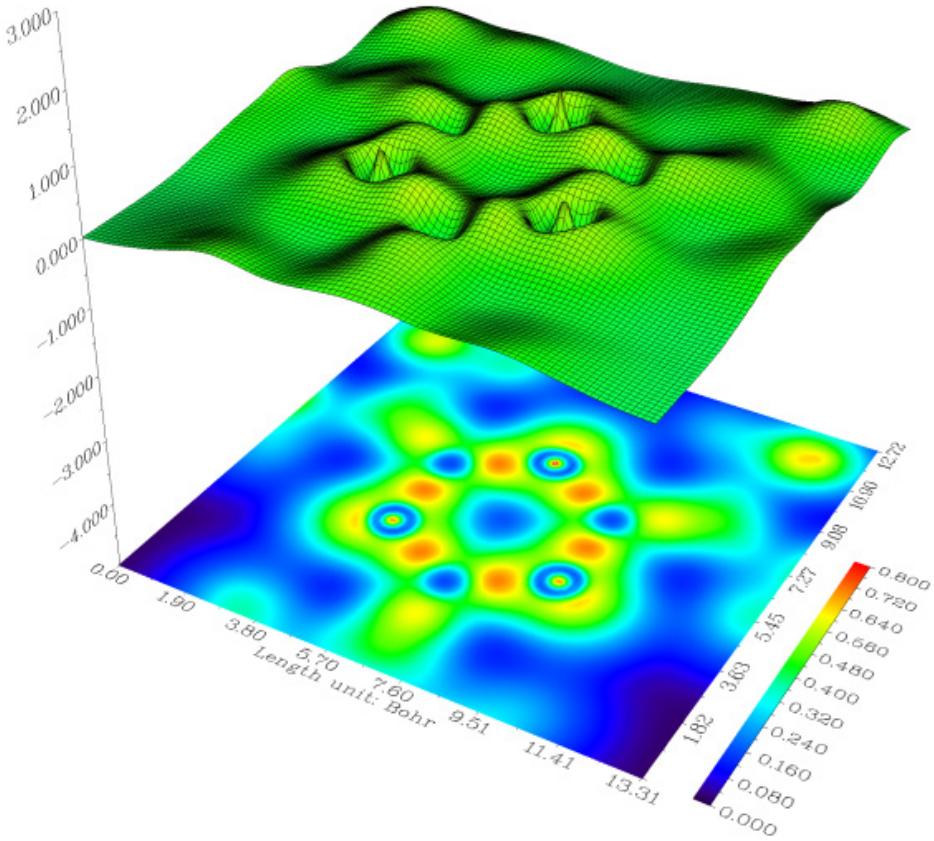

Fig. 3. ELF snapshot of ALT molecule interaction with Fe^{2+}.

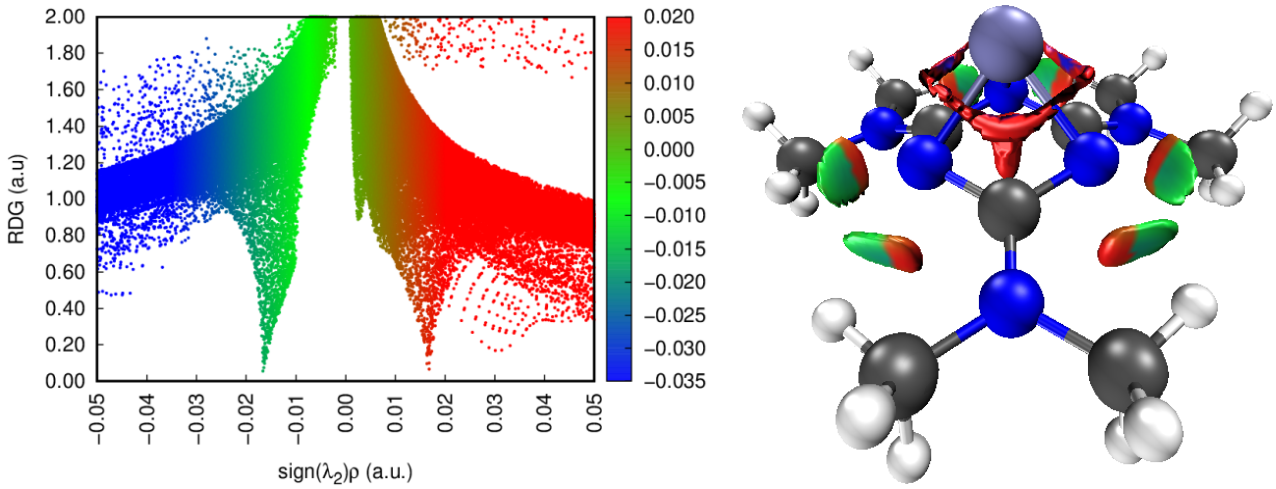

Fig. 4. Reduced density gradient iso-surface map of the ALT···Fe^{2+} complex.

Table 2. The selected topological properties of electron density (in a.u.) obtained by AIM analysis.

	ρ_{BCP}	$\nabla^2\rho_{BCP}$	H	G	V	-G/V	ε	$\lvert\lambda_1\rvert/\lambda_3$
Fe^{2+}	0.0977	0.3889	-0.0236	0.1202	-0.1438	0.8357	0.3280	0.1075
Zn^{2+}	0.0633	0.1907	-0.0150	0.0629	-0.0782	0.8046	0.1884	0.0629
Si^{2+}	0.0739	0.0359	-0.0410	0.0497	-0.0904	0.5496	0.0492	0.0690
Ge^{2+}	0.0668	0.1058	-0.0200	0.0462	-0.0660	0.7004	0.0490	0.0644
Mg^{2+}	0.0350	0.1873	0.0034	0.0434	-0.0400	1.0852	0.1918	0.0348
Ca^{2+}	0.0345	0.1363	0.0020	0.0321	-0.0301	1.0663	0.2288	0.0336

3.4. NBO analysis

In this method, we evaluate the effects of delocalization between the donor and acceptor orbitals [81]. For each donor NBO (i) and acceptor NBO (j), the stabilization energy, $E^{(2)}$, related to the delocalization of i → j, is defined as follows:

$$E^{(2)} = -q_i \frac{(F_{i,j})^2}{\varepsilon_j - \varepsilon_i} \quad (4)$$

where q_i is the orbital occupancy, ε_i and ε_j denote diagonal elements, and F(i,j) indicates the off-diagonal NBO Fock matrix elements [81]. Table 3 shows the results of the NBO analysis in the corresponding complexes. According to the data, the key interactions in the selected complexes occur between the bonding orbitals (or lone pairs) of the donor species with the anti-bonding orbitals (or anti-bonding lone pairs) of the acceptor groups.

The amounts of donor-acceptor energies, $E^{(2)}$, obtained are in the range of 0.52-5.13 kcal/mol. Our data display that the maximum and minimum values of $E^{(2)}$ belong to the Fe^{2+} and Ca^{2+} complexes, respectively. As a result, the charge transfer from donor species to acceptor groups is larger in the first case than in the second case. Furthermore, the $E^{(2)}$ values can give qualitative information about the intensity of binding energies (Table 1 and 3). For each ionic group, these results follow the same trend as the $\Delta E_{ion-\pi}$ and ρ_{BCP} values. This indicates that charge transfer can be an appropriate feature in assessing the strength of cation-π interactions.

The NBO analysis also evaluates the allocation of atomic charges, s-character percentage of $\sigma_{(C-N)}$, and p-character proportion of the Fe^{2+} and Ca^{2+} cations in the ALT···Fe^{2+} and ALT···Ca^{2+} complexes. Theoretical predictions suggest that the p-character of LP^*_{Fe2+} ($sp^{1.00}$) is greater than that of the LP^*_{Ca2+} ($sp^{0.06}$). Furthermore, the $d_{ion-\pi}$ distance of the ALT···Fe^{2+} complex (1.603 Å) is less than that of ALT···Ca^{2+} (2.163 Å). Our findings confirm that the $d_{ion-\pi}$ is primarily affected by the p-character of the hybrid orbitals. Moreover, the s-character proportion in the C-N bonding orbitals (σ_{C-N}) reduces in the ALT···Ca^{2+} (34.62%) when compared to the ALT···Fe^{2+} (38.08%). These results show that the ALT···Fe^{2+} complex requires more energy than the ALT···Ca^{2+}.

3.5. Aromaticity analysis

The aromaticity of the complexes is assessed using two widely recognized indices: the HOMA and the FLU. These aromaticity indices are calculated using the Multiwfn 3.7 program [85], which facilitates detailed evaluation of the electronic structure and aromatic character of the molecules [90]. Both HOMA and FLU offer complementary insights. HOMA focuses on geometric parameters related to bond lengths, while FLU measures fluctuations in electron delocalization, providing a robust quantification of aromaticity. The

HOMA index is evaluated by a scale ranging from 0 to 1. A value of 1 signifies complete delocalization within aromatic rings, while a value of zero indicates total localization. An analysis of Table 4 reveals that, except for the complexes with transition ions, the ALT complexes with Ge^{2+} and Ca^{2+} exhibit greater aromaticity compared to those with Si^{2+} and Mg^{2+}. This demonstrates a greater impact on aromaticity in the former complexes compared to the latter. As a result, aromaticity values are influenced by the nature of the cations.

Table 4 also shows that in each ion group, the ALT···M complexes (M = Zn^{2+}, Ge^{2+}, and Ca^{2+}) have the lowest FLU indices. It is well-known that for more aromatic species, the FLU values are close to zero. According to the findings, in most cases, the results of indices are similar, indicating that complexes with a higher HOMA index have a lower FLU index. The relationship among aromaticity indices and cation-π interaction parameters can also be considered. The results demonstrate that both aromaticity indices exhibit good linear connections with $\Delta E_{ion\text{-}\pi}$, with correlation coefficients (R) greater than 0.8. Based on these findings, the strength of the cation-π interaction can be estimated using aromaticity indices.

The one-electron characteristics, such as dipole moment and polarizability, are also evaluated on the complexes. The dipole moment is defined as the first derivative of the energy with respect to an applied electric field [91]. Table 4 shows the obtained dipole moment (μ°) values in the complexes. The results show that the dipole moment values range from 0.04 to 8.84 D. For each ionic group, the dipole moments increase for the Zn^{2+}, Ge^{2+}, and Ca^{2+} complexes, with the highest value observed for the Ca^{2+} complex. On the other hand, the smallest dipole moments are observed in the Fe^{2+}, Si^{2+}, and Mg^{2+} complexes, with the lowest value being detected for the Fe^{2+} complex. This indicates that the dipole moments of different complexes depend on the nature of the selected metal cations. Polarizability is defined as the second derivative of energy with respect to the applied electric field [91]. The results show that a similar trend exists between the dipole moment and the polarizability of complexes (Table 4).

Garau et al. [92] showed that molecules with small permanent quadrupole moment values, Q_{zz}, can interact acceptably with cations. The presence of different cations influences the aromatic ring's π-electron density, leading to an increase (or decrease) in the quadrupole moment of the π-system. Our findings show that, in most cases, there are significant relationships among the dipole moment, polarizability, and quadrupole moment of the complexes, such that the values of these parameters are greater in complexes with weaker binding energy than in those with higher energy (Table 4). This means that these quantities exert the same effects on the interaction between the ALT system and the selected metal cations.

3.6. Electronic properties

Using frontier molecular orbital (FMO) theory, the electronic properties of the designed complexes can be determined. The nucleophilic and electrophilic properties of compounds are attributed to their molecular orbitals (HOMO and LUMO). The energy gap between these orbitals determines the kinetic stability and chemical reactivity of these compounds ($E_g = E_{LUMO} - E_{HOMO}$). A large energy gap means that the system has high stability and consequently low reactivity, and vice versa. Figure 5 shows a diagram of the HOMO and LUMO molecular orbitals and their energy gap for the ALT···Fe^{2+} complex. The quantities related to the chemical reactivity of the complexes collected in Table 5 are defined as follows:

$$\mu = \left(\frac{\partial E}{\partial N}\right)_{V(r),T} \quad (6)$$

$$\eta = \left(\frac{\partial^2 E}{\partial N^2}\right)_{V(r),T} \quad (7)$$

$$S = \frac{1}{\eta} \quad (8)$$

$$\omega = \frac{\mu^2}{2\eta} \quad (9)$$

where chemical potential (μ) [93], chemical hardness (η) [94], global softness (S), and electrophilicity index (ω) [95] are described as conceptual DFT parameters. In an N-electron system, μ and η are defined as the first and second derivatives of the total energy relative to the external potential, respectively. Softness is the inverse of hardness, which estimates the molecule's polarizability and the ease of charge transfer. The electrophilicity index is also determined based on the electrophilic nature of the compounds.

The results in Table 5 show that the maximum energy gap is for the Si^{2+} complex, while the minimum amount is for the Zn^{2+} complex. These results confirm increased stability in the former complex and greater reactivity in the latter complex. To prove our analysis, energy gaps are also calculated with the PBE0 functional (Table 5). The results show a similar trend to the obtained results at the ωB97XD/6-311++G(d,p) level of theory. There is a direct relationship between the energy gap values and chemical hardness. Negative values of the chemical potential confirm the stability of all complexes (see Table 5).

The electronegativity value is proportional to the negative chemical potential ($\chi = -\mu$) [96]. In the complexes studied, the highest electronegativity is observed in the ALT···Zn^{2+} complex; hence, this compound is the best electron acceptor.

The energy gaps of large and small are associated with the hard and soft molecules, respectively.

Table 3. Values of second-order perturbation energy ($E^{(2)}$, in kcal mol^{-1}) and occupation numbers of donor ($O.N._D$) and acceptor ($O.N._A$) orbitals.

	Donor orbital	Acceptor orbital	$E^{(2)}$	$O.N._D$	$O.N._A$
Fe^{2+}	BD(1)C-N	LP*(Fe^{2+})	4.43	1.9681	0.0157
	LP(1)N	LP*(Fe^{2+})	5.13	1.8769	0.0272
Zn^{2+}	BD(1)C-N	LP*(Zn^{2+})	2.05	1.9772	0.0132
Si^{2+}	BD(1)C-N	BD*(1)N-Si	1.48	1.9725	0.0138
	LP(1)N	RY*(Si^{2+})	0.62	1.913	0.0028
Ge^{2+}	BD(1)C-N	BD*(1)N-Ge	0.83	1.9759	0.0122
Mg^{2+}	BD(1)C-N	LP*(Mg^{2+})	1.30	1.9779	0.0482
	LP(1)N	LP*(Mg^{2+})	0.59	1.9048	0.0482
Ca^{2+}	BD(1)C-N	LP*(Ca^{2+})	0.56	1.9803	0.0275
	LP(1)N	LP*(Ca^{2+})	0.52	1.9007	0.0275

Table 4. Calculated aromaticity indices, values of the dipole moment (μ°, in Deby), quadrupole moment (Q_{ZZ}, in B) and polarizability (in B^3) of ALT···M complexes.

	HOMA	FLU	μ° (D)	Q_{ZZ}	Polarizability
Fe^{2+}	0.6923	0.1268	0.04	-76.76	166.76
Zn^{2+}	0.6695	0.0997	1.39	-73.02	174.67
Si^{2+}	0.6360	0.1004	1.15	-83.58	170.98
Ge^{2+}	0.6847	0.0948	1.38	-81.86	174.06
Mg^{2+}	0.7465	0.0778	6.96	-58.88	163.76
Ca^{2+}	0.8816	0.0570	8.84	-59.49	168.33

Table 5. Values of the HOMO and LUMO energies (E_{HOMO} and E_{LUMO}), energy gap (E_g), chemical hardness (η), electronic chemical potential (μ), electronegativity (χ), softness (S), and electrophilicity index (ω) of ALT complexes.

	E_{HOMO} (eV)	E_{LUMO} (eV)	E_g (eV)	η (eV)	μ (eV)	χ (eV)	S (eV^{-1})	ω (eV)
Fe^{2+}	-16.760	-8.116	8.644 (4.895)[a]	4.322	-12.438	12.438	0.231	17.898
Zn^{2+}	-16.547	-10.210	6.340 (2.958)	3.170	-13.377	13.377	0.315	28.225
Si^{2+}	-16.619	-7.217	9.402 (5.928)	4.701	-11.918	11.918	0.213	15.108
Ge^{2+}	-16.585	-7.713	8.872 (5.452)	4.436	-12.149	12.149	0.225	16.636
Mg^{2+}	-16.215	-8.865	7.350 (3.571)	3.675	-12.540	12.540	0.272	21.394
Ca^{2+}	-15.604	-7.433	8.171 (4.629)	4.085	-11.519	11.519	0.245	16.239

[a] Values in parentheses refer to the estimated energy gaps in the PBE0 level of theory.

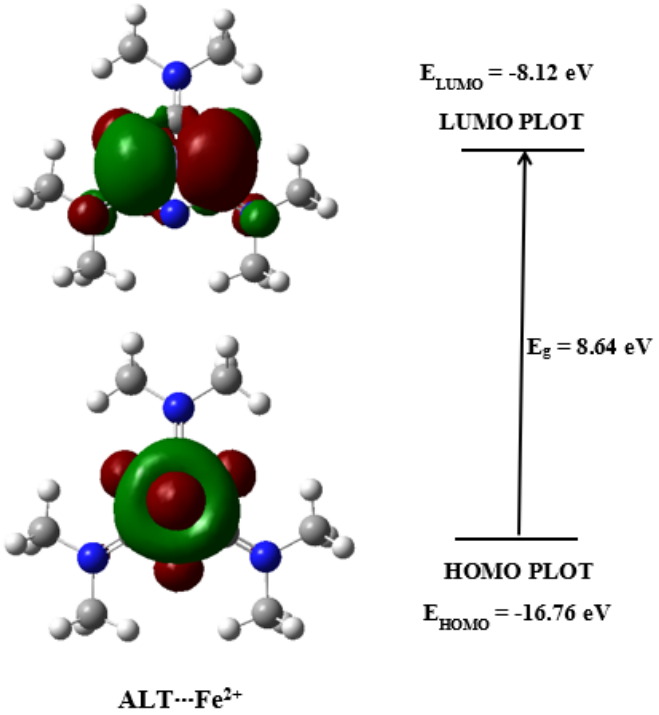

Fig. 5. HOMO and LUMO plot of ALT···Fe^{2+} complex obtained at the ωB97XD/6-311++G(d,p) level of theory.

Soft molecules are more polarizable than hard ones because they require less energy to excite. The results in Table 5 show that the most reactive complex belongs to ALT···Zn^{2+}, which has the highest chemical softness. There is an inverse relationship between the HOMO-LUMO energy gap and the softness of the complexes. In other words, reduction of the energy gap is accompanied by an increase in softness.

Figure 6 shows the linear relationship between the energy gap and the softness of the complexes.

The electrophilicity index (ω) also evaluates the chemical reactivity of complexes.

It is classified into three groups based on the electrophilic nature of the structures: weak, medium, and strong electrophiles, and are shown as ω < 0.8 eV, 0.8 < ω < 1.5 eV, and ω > 1.5 eV [95, 97], respectively. According to the results, the lowest energy gap leads to the highest electrophilicity, and vice versa.

Our findings in Table 5 show that the highest electrophilicity index is for the Zn^{2+} complex, and the lowest value is for the Si^{2+} complex. It is in agreement with previous results.

This means that the electrophilic nature of the former complex is greater than the latter.

3.7. Electrostatic potential

In intermolecular interactions, the effective localization of electron density within a molecule, the charge distribution, shape, and size of structures can be visualized through molecular electrostatic potential (MPE) maps [98, 99].

Nucleophilic and electrophilic reaction sites are evaluated with this method. The electron density isosurface of the ALT···Fe^{2+} complex computed using the ωB97XD method and the 6-311++G(d,p) basis set is shown in Figure 7 On the MPE surface, the electron-rich and electron-poor regions are depicted in red and blue, respectively. The neutral electrostatic potential is represented in green. As shown in Figure 7, electron-poor areas are located on the Fe^{2+} cation and the plane of the aromatic ring (blue), which can participate in nucleophilic attacks.

3.8. Nuclear magnetic resonance (NMR) analysis

In this section, the values of the nitrogen shielding (N shielding) tensor, along with coupling constants ($^1J_{C-N}$) of the complexes, are computed. Some NMR data acquired at the ωB97XD/6-311++G(d,p) level are displayed in Table 6.

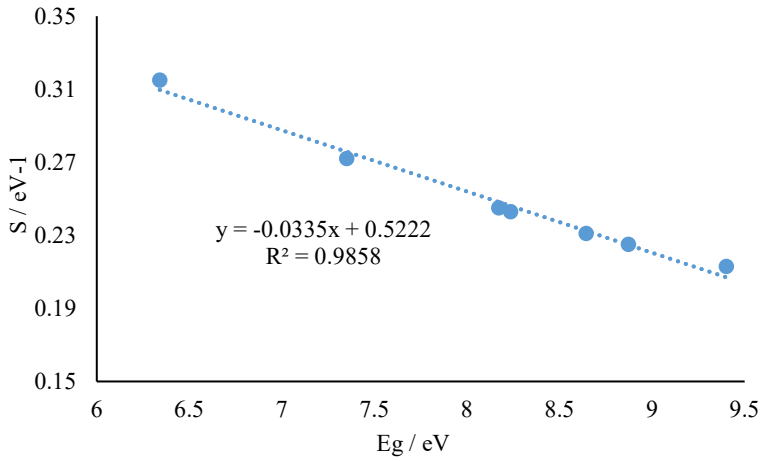

Fig. 6. Correlation between the softness (S) and the energy gap (E_g) for the ALT···M complexes.

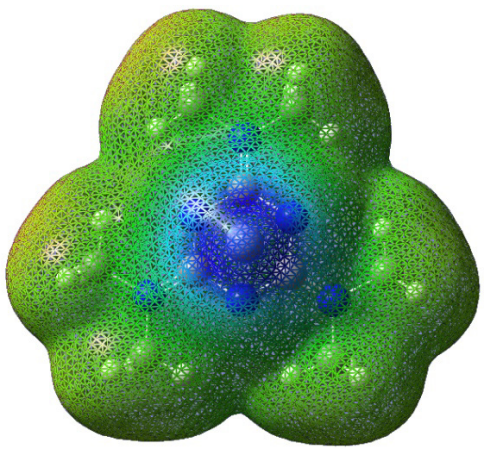

Fig. 7. Electron density isosurface of ALT···Fe^{2+} complex calculated by ωB97XD method and 6-311++G(d,p) basis set.

Table 6. Some NMR data calculated at the ωB97XD/6-311++G(d,p) level of theory.

	N shielding (ppm)	δ^N (ppm)	$^1J_{C\text{-}N}{}^a$ (Hz)	$^1J_{C\text{-}N}{}^b$ (Hz)	FC	SD	PSO	DSO	FC	SD	PSO	DSO
					$^1J_{C-N}{}^a$				$^1J_{C-N}{}^b$			
Fe^{2+}	311.98	-280.22	-0.76	21.74	0.92	0.05	-1.88	0.15	24.43	0.95	-3.77	0.13
Zn^{2+}	60.63	-28.87	-0.17	22.25	1.35	0.13	-1.79	0.15	24.78	1.16	-3.83	0.13
Si^{2+}	78.68	-46.92	0.26	22.05	1.79	0.03	-1.69	0.13	24.65	1.15	-3.87	0.12
Ge^{2+}	75.32	-43.56	0.37	22.13	1.96	0.05	-1.78	0.15	24.75	1.04	-3.79	0.13
Mg^{2+}	102.11	-70.35	-0.18	21.81	1.66	0.02	-1.98	0.12	24.45	0.87	-3.62	0.12
Ca^{2+}	78.88	-47.12	1.20	21.40	3.35	0.02	-2.30	0.13	23.98	0.62	-3.32	0.13

[a] Cyclic C—N coupling constant. [b] Exocyclic C—N coupling constant

Examination of NMR data and binding energies shows the significant relationships between them (see Table 1 and 6). In each ion group, stronger binding energies of the complexes lead to an increase in the isotropic of the N shielding tensors.

Thus, the highest $|\Delta E_{ion\text{-}\pi}|$ value corresponds with the greatest N shielding. The calculated chemical shifts of nitrogen atoms (δ^N) within the ALT complexes are also presented in Table 6. The findings indicate that as the values of the N shielding tensors increase, the chemical shifts of this atom decrease. Consequently, the relationships between N shielding and the $d_{ion-\pi}$, $\Delta E_{ion\text{-}\pi}$, and ρ values computed at the BCP are inverted when substituting N shielding with chemical shifts.

The influence of the cation-π interaction on the spin-spin coupling constants of $^1J_{C\text{-}N}$ (cyclic and exocyclic) is also examined in this framework (refer to Table 6). As shown in this table, for each ion group, the $^1J_{C\text{-}N}$ (cyclic) of the Zn^{2+}, Ge^{2+}, and Ca^{2+} complexes increases relative to the Fe^{2+}, Si^{2+}, and Mg^{2+} complexes. Similar results are also observed for $^1J_{C\text{-}N}$ values of exocyclic. (except for group IIA ions). Our findings establish that, in most cases, $^1J_{C\text{-}N}$ values and $|\Delta E_{ion\text{-}\pi}|$ exhibit contrasting trends. This implies that coupling constants could be valuable indicators in evaluating the cation-π interactions of the selected complexes.

There are 4 components for the total spin-spin coupling constant, including the paramagnetic spin-orbit (PSO), diamagnetic spin-orbit (DSO), Fermi contact (FC), and spin-dipole (SD) terms [100-102]. The results are collected in Table 6. According to the obtained data, the Fermi contact term is the most important component, and its trend is identical to $^1J_{C\text{-}N}$ (cyclic). Also, the diamagnetic spin-orbit term is constant and does not change with the transition metal complexes, while a direct relationship exists between these values and $^1J_{C\text{-}N}$ in the other complexes. In the cation-π complexes, the decrease in the value of $^1J_{C\text{-}N}$ is accompanied by an increase in the value of the paramagnetic spin-orbit (except for Fe^{2+} and Zn^{2+} complexes). The direct order between the spin-dipole term in these complexes and its order in $^1J_{C\text{-}N}$ is present.

The components of $^1J_{C\text{-}N}$ (exocyclic) are also collected in Table 6. The calculations show that the FC term is also the most important factor in $^1J_{C\text{-}N}$. Because the SD, DSO, and PSO terms are negligible compared to the values of the FC term. Our findings show that the order of the FC term is similar to $^1J_{C\text{-}N}$. No meaningful relationships can be observed between $^1J_{C\text{-}N}$ values and PSO or SD terms. Also, the DSO term is nearly constant and does not change with the different complexes.

4. Conclusion

In this work, the evaluation of cation-π interactions between the ALT drug and Fe^{2+}, Zn^{2+}, Si^{2+}, Ge^{2+}, Mg^{2+}, and Ca^{2+} cations is carried out in the gas phase and solution. Results show that the binding strength in the gas phase is higher than in the solution.

In the gas phase, the highest binding energy is observed for the Fe^{2+} complex, whereas in solution, it is detected for the Si^{2+} complex. According to the results, cation-π interactions in the complexes are of a closed-shell nature. In complexes with transition metal ions and quasi-metal ions, because of their negative H values, they have a partially covalent nature.

On the other hand, the group IIA metal complexes exhibit a non-covalent character. The results of NBO analysis show that the maximum and minimum values of $E^{(2)}$ belong to the Fe^{2+} and Ca^{2+} complexes, respectively. As a result, the charge transfer from donor species to acceptor groups is larger in the first case than in the second case. Moreover, for each ion group, the $E^{(2)}$ values have an identical trend with $\Delta E_{ion\text{-}\pi}$ and ρ_{BCP} values.

According to the aromaticity analyses, in most cases, the results of indices are similar, indicating that complexes with a higher HOMA index have a lower FLU index. In general, there are significant relationships among the dipole moment, polarizability, and quadrupole moment of the complexes, such that the values of these parameters are greater in complexes with weaker binding energy than in those with higher energy. This means that these quantities exert the same effects on the interaction between the ALT system and the selected metal cations.

Results of the FMO analysis show that the maximum energy gap is for the Si^{2+} complex, while the minimum value is for the Zn^{2+} complex. These results confirm increased stability in the former complex and greater reactivity in the latter complex. The results of NMR analysis show that, for each ion group, stronger binding energies lead to an increase in the

isotropic of the N shielding tensors. The findings also indicate that as the values of the N shielding tensors increase, the chemical shifts of this atom decrease. Consequently, the relationships between N shielding and the $d_{ion-\pi}$, $\Delta E_{ion-\pi}$, and ρ values computed at the BCP are inverted when substituting N shielding with chemical shifts. This computational study holds strong promise for advancing pharmaceutical chemistry by revealing metal-specific structural and electronic modulations that could enhance the drug's anticancer efficacy. The findings lay the groundwork for designing metal-altretamine conjugates with tailored stability and reactivity, potentially improving bioavailability or targeting in chemotherapy.

Quasi-metal complexes (Si^{2+}, Ge^{2+}) may introduce unique covalent bonding traits, opening avenues for novel nanomaterials or hybrid therapeutics. This work contributes to rational drug design in metal-drug interactions, fostering interdisciplinary links between quantum chemistry and oncology for next-generation altretamine derivatives.

Acknowledgements

The authors wish to thank Payame Noor University, Tehran, Iran, for their support.

References

[1] B.J. Foster, K. Clagett-Carr, S. Marsoni, R. Simon, B. Leyland-Jones, Role of hexamethylmelamine in the treatment of ovarian cancer: Where is the needle in the haystack? *Cancer Treat. Rep.*, 70 (1986) 1003–1014.

[2] J.F. Worzalla, B.M. Johnson, G. Ramirez, G.T. Bryan, N-Demethylation of the antineoplastic agent hexamethylmelamine by rats and man. *Cancer Res.*, 33 (1973) 2810–2815.

[3] B.J. Foster, B.J. Harding, B. Leyland-Jones, D. Hoth, Hexamethylmelamine: A critical review of an active drug. *Cancer Treat. Rev.*, 13 (1986) 197–217.

[4] J. Dubois, R. Arnould, F. Abikhalil, M. Hanocq, G. Atassi, G. Ghanem, et al., In vitro cytotoxicity of hexamethylmelamine (HMM) and its derivatives. *Anticancer Res.*, 10 (1990) 827–832.

[5] B. Gidwani, A. Vyas, Preparation, characterization, and optimization of altretamine-loaded solid lipid nanoparticles using Box-Behnken design and response surface methodology. *Artif. Cells Nanomed. Biotechnol.*, 44 (2016) 571-580.

[6] M.M. Torrice, K.S. Bower, H.A. Lester, D.A. Dougherty, Probing the role of the cation–π interaction in the binding sites of GPCRs using unnatural amino acids. *Proc. Natl. Acad. Sci. U. S. A.*, 106 (2009) 11919-11924.

[7] F. Alirezapour, M. Mohammadi, A. Khanmohammadi, Exploration of the mutual effects between cation–π and intramolecular hydrogen bond interactions in the different complexes of mesalazine with metal cations of alkali and alkaline earth: a DFT study. *Chem. Rev. Lett.*, 6 (2023) 262–275. https://doi.org/10.22034/crl.2023.415348.1245

[8] M.J.Z. Sagheb, L. Hokmabady, A. Khanmohammadi, A comprehensive investigation into the effect of substitution on electronic structure, charge transfer, resonance, and strength of hydrogen bond in 3–amino-propene thial and its analogous: A DFT calculation. *Chem. Rev. Lett.*, 6 (2023) 308–326. https://doi.org/10.22034/crl.2023.416216.1248

[9] H. Bahir, S.K. Mohammed, A.M. Ibrahim, A.A. Hussein, A. Khanmohammadi, A theoretical study of X–H···C and X–H···π interactions between substituted benzene derivatives and HF, HCl and HBr: AIM, NBO and NMR analyses. *Chem. Rev. Lett.*, 6 (2023) 479–493. https://doi.org/10.22034/crl.2023.416728.1249

[10] A.S. Isa, A. Uzairu, U.M. Umar, M.T. Ibrahim, A.B. Umar, QSAR, docking and pharmacokinetic studies of 2,4-diphenyl indenol [1,2-B] pyridinol derivatives targeting breast cancer receptors. *J. Chem. Lett.*, 5 (2024) 44–57. https://doi.org/10.22034/jchemlett.2024.424800.1146

[11] A.I. Kubo, N.A. Jibrilla, A. Elijah, M. Sani, A.S. Isa, Y.A. Sidi, et al., Insight into Pharmacokinetic and Drug-likeness Properties: Predictive Modelling of 1,9-Diheteroarylnona-1,3,6,8-Tetraen-5-Ones Derivatives as Prostate Cancer Therapeutic Agent Targeting (1z8l) Protein Receptor. *Med. Med. Chem.*, 1 (2025) 163–172. https://doi.org/10.22034/medmedchem.2025.494085.1024

[12] A.S. Isa, A.M. Mohammed, Computational Analysis of Novel 4-Thiazolidinone Derivatives as Potential Anti-Breast Cancer Agents: Docking, Pharmacokinetics, and Molecular Dynamics Study. *Med. Med. Chem.*, 1 (2024) 102–114. https://doi.org/10.22034/medmedchem.2024.488996.1015

[13] C.I. Aghanwa, U.E. Ekpunobi, A.S. Ogbuagu, Bioactive Constituents Interactions with 5-HT2C and PDE-5 Receptors in Herbal Drug Mixtures used in the treatment Of Premature Ejaculation sold in Anambra State, Nigeria. *Med. Med. Chem.*, 1 (2024) 44–63. https://doi.org/10.22034/medmedchem.2024.480097.1013

[14] N. Zacharias, D.A. Dougherty, Cation–π interactions in ligand recognition and catalysis. *Trends Pharmacol. Sci.*, 23 (2002) 281-287.

[15] D.T. Infield, A. Rasouli, G.D. Galles, C. Chipot, E. Tajkhorshid, C.A. Ahern, Cation-π interactions and their functional roles in membrane proteins. *J. Mol. Biol.*, 433 (2021) 167035.

[16] T. Yadollahi, R. Ghiasi, S. Baniyaghoob, Unveiling of interactions of ansa-titanocene dichloride and ansa-vanadocene dichloride anticancer drugs with B12N12 cage. *Inorg. Chem. Commun.*, 173 (2025) 113896.

[17] R. Ghiasi, M. Nikbakht, H. Pasdar, Interactions of the potential antitumor agent vanadocene dichloride with C20 and M+@C20 (M= Li, Na, K) nano-cages: A DFT investigation. *Results Chem.*, 9 (2024) 101659.

[18] R. Ghiasi, M. Nikbakht, A. Amiri, Understanding the interactions between anticancer active molecules Cp2TiCl2 and Cp2VCl2 and E@Al12 (E=C, Si) cluster using density functional theory calculations. *Inorg. Chem. Commun.*, 164 (2024) 112446.

[19] A. Solgi, R. Ghiasi, S. Baniyaghoob, PCM, ETS-NOCV, and CDA investigations of interactions of a cycloplatinated thiosemicarbazone as antiparasitic and antitumor agents with C20 nano-cage. *Int. J. Nano Dimens.*, 14 (2023) 219-226.
[20] R. Ghiasi, A. Valizadeh, Computational investigation of interaction of a cycloplatinated thiosemicarbazone as antitumor and antiparasitic agents with B12N12 nano-cage. *Results Chem.*, 5 (2023) 100768.
[21] Z. Liang, Q.X. Li, π-Cation interactions in molecular recognition: perspectives on pharmaceuticals and pesticides. *J. Agric. Food Chem.*, 66 (2018) 3315–3323.
[22] R. Ghiasi, A. Valizadeh, Interaction of cisplatin anticancer drug with C20 bowl: DFT investigation. *Main Group Chem.*, 21 (2022) 43–54.
[23] M. Shabani, R. Ghiasi, K. Zare, R. Fazaeli, Computational investigation of interaction between titanocene dichloride and nanoclusters (B12N12, B12P12, Al12N12 and Al12P12). *Main Group Chem.*, 20 (2021) 437-446.
[24] M. Shabani, R. Ghiasi, K. Zare, R. Fazaeli, The interaction between carboplatin anticancer drug and B12N12 nano-cluster: A computational investigation. *Main Group Chem.*, 20 (2021) 345–354.
[25] R. Ghiasi, M. Vasfi Sofiyani, R. Emami, Computational investigation of interaction of titanocene dichloride anti-cancer drug with carbon nanotube in presence of external electric field. *Biointerface Res. Appl. Chem.*, 11 (2021) 12454-12461.
[26] R. Ghiasi, M. Rahimi, Complex formation of titanocene dichloride anticancer and Al12N12 nano-cluster: a quantum chemical investigation of solvent, temperature and pressure effects. *Main Group Chem.*, 20 (2021) 19–32.
[27] A. Zaboli, H. Raissi, F. Farzad, H. Hashemzadeh, F. Fallahi, Cation-π interaction: A strategy for enhancing the performance of graphene-based drug delivery systems. *Inorg. Chem. Commun.*, 141 (2022) 109542.
[28] A. John, A. Uzairu, G.A. Shallangwa, S. Uba, Theoretical Investigation and Design of Novel Cephalosporin Based Inhibitors of a DD-carboxypeptidase Enzyme of Salmonella typhimurium. *J. Chem. Lett.*, 4 (2023) 52–58. https://doi.org/10.22034/jchemlett.2022.361586.1085
[29] B. Singh, A.K. Suman, Tetrazole containing 1,5-benzothiazepines: Design, synthesis, in silico and in vitro evaluation as medicinally potent ACE inhibitors. *J. Chem. Lett.*, 5 (2024) 192–205. https://doi.org/10.22034/jchemlett.2024.468311.1214
[30] L.V.R. Lakshmidevi, V.B, S.K.C. Swathy, A. Chandran E, Design synthesis and in vitro anticancer activity of novel imidazolyl benzoic acid derivatives. *J. Chem. Lett.*, 6 (2025) 135–141. https://doi.org/10.22034/jchemlett.2025.486896.1243
[31] J.T. Mehrabad, F.A. Rad, E.D. Maleki, Synthesis and characterization of Gabapentin-Zn_2Al-LDH nanohybrid and investigation of its drug release and biocompatibility properties on a laboratory scale. *J. Chem. Lett.*, 5 (2024) 71–78. https://doi.org/10.22034/jchemlett.2024.442139.1157
[32] A.B. Adam, M.Y. Abubakar, D. Abubakar, Green Organic Synthesis in Drug Development: Advances in Enzyme- and Microorganism-Mediated Processes. *Med. Med. Chem.*, 1 (2024) 115–128. https://doi.org/10.22034/medmedchem.2024.489545.1017
[33] R.M. Mhaibes, P.G. Dastnaei, M.R.J. Sarvestani, Recent Developed Drug Delivery Systems. *Med. Med. Chem.*, 1 (2024) 156–162. https://doi.org/10.22034/medmedchem.2024.475043.1009
[34] E. Vaziri, K.J. Rad, A. Mohasseb, A Comprehensive Review on Levodopa Pharmacology and Its Drug Delivery Methods. *J. Chem. Technol.*, 1 (2025) 1–6. https://doi.org/10.22034/jchemtech.2025.530588.1008
[35] A.B. Adam, A. Aneshi, D. Filibus, M.Y. Abubakar, A. Bilyaminu, Nano-Enabled Analytical Chemistry: Application in Targeted Drug Delivery and Diagnostics. *J. Med. Med. Chem.*, 1 (2025) 73–80. https://doi.org/10.22034/jmedchem.2025.533514.1008
[36] C. Jones, J. Thornback, *Medicinal applications of coordination chemistry*, RSC Publishing, Cambridge (2007).
[37] D. Arthur, G.B. Dogara, A.A. Babafem, J.C. Akan, Computational Modeling of Chemical Inhibitors Targeting the HIV-1 Main Protease: A Review. *Med. Med. Chem.*, 1 (2024) 71–83. https://doi.org/10.22034/medmedchem.2024.485335.1014
[38] A.S. Isa, A.K. Ibrahim, A.M. Mukhtar, In silico Analysis, Anti-Proliferative Activity Modeling, Molecular Docking and Pharmacokinetic Properties Prediction of Some Tetrahydropyrazole-Quinazoline Derivatives as Cancer Therapeutic Agents. *Med. Med. Chem.*, 1 (2025) 138–155. https://doi.org/10.22034/medmedchem.2025.492523.1022
[39] S.N. Adawara, A.S. Isa, F.A. Yaro, M.A. Tijjani, U.T. Mamza, M. Iji, et al., Triazolopyrimidine Derivatives for Cancer: An In Silico Evaluation of Docking and Pharmacokinetics. *J. Chem. Technol.*, 1 (2025) 116–125. https://doi.org/10.22034/jchemtech.2025.539505.1016
[40] A. Mohasseb, K.J. Rad, A Review on Fluphenazine Pharmacology and its Analytical Methods. *J. Med. Med. Chem.*, 1 (2025) 24–29. https://doi.org/10.22034/jmedchem.2025.526832.1005
[41] M. Roney, M.F.F.M. Aluwi, Anti-diabetic Activity of Phloretin Against Maltase-glucoamylase Using Docking, Pharmacokinetics and Pharmacophore Studies. *J. Chem. Lett.*, 4 (2023) 164–170. https://doi.org/10.22034/jchemlett.2023.411216.1131
[42] O.J. Anekwe-Nwekeaku, E.J. Morah, O.C. Ezeigwe, E.C. Ezeudu, A.I. Obi, N.V. Nwankwo, Extensive study on the pharmaceutical constituents of leaf and root of Costus after (ker). *J. Chem. Lett.*, 5 (2024) 168–185. https://doi.org/10.22034/jchemlett.2024.453754.1183
[43] M.R.J. Sarvestani, P.G. Dastnaei, A Review on Mesna Pharmacology and its Analytical Techniques. *Med. Med. Chem.*, 1 (2024) 31–35. https://doi.org/10.22034/medmedchem.2024.474838.1004
[44] M.R.J. Sarvestani, Potentiometric Sensors Developed for the Measurement of Pharmaceutical Compounds. *Med. Med. Chem.*, 1 (2024) 84–90. https://doi.org/10.22034/medmedchem.2024.475078.1010
[45] N. Mirderikvand, M. Mahboubi-Rabbani, Adsorptive Removal of Neomycin by Schiff Base Network1 (SNW1) Covalent Organic Framework. *J. Chem. Technol.*, 1 (2025) 47–51. https://doi.org/10.22034/jchemtech.2025.538158.1013
[46] T. Loftsson, Drug solubilization by complexation. *Int. J. Pharm.*, 531 (2017) 276-280.

[47] R. Ghiasi, R. Emami, M. Vasfi Sofiyani, Interaction between carboplatin with B12P12 and Al12P12 nano-clusters: A computational investigation. *Phosphorus Sulfur Silicon Relat. Elem.*, 196 (2021) 751–759.

[48] M. Shabani, R. Ghiasi, K. Zare, R. Fazaeli, Quantum chemical study of interaction between titanocene dichloride anticancer drug and Al12N12 nano-cluster. *Russ. J. Inorg. Chem.*, 65 (2020) 1726–1734.

[49] (a) S. Kumar, S. Zhou, S.K. Singh, Metal ion leachates and the physico-chemical stability of biotherapeutic drug products. *Curr. Pharm. Des.*, 20 (2014) 1173-1181; (b) S. Esfahani, J. Akbari, S. Soleimani-Amiri, Adsorption of ibuprofen by an iron-doped silicon carbide graphene monolayer: DFT exploration of drug delivery insights. *Int. J. Nano Dimens.*, 15 (2024) 63-71.

[50] (a) Z. Kazemi, R. Ghiasi, S. Jamehbozorgi, Analysis of the interaction between the C20 cage and cis-PtCl2(NH3)2: a DFT investigation of the solvent effect, structures, properties, and topologies. *J. Struct. Chem.*, 59 (2018) 1044-1051; (d) S. Esfahani, J. Akbari, S. Soleimani-Amiri, M. Mirzaei, A. Ghasemi Gol, et al., Assessing the drug delivery of ibuprofen by the assistance of metal-doped graphenes: Insights from density functional theory. *Diam. Relat. Mater.*, 135 (2023) 109893.

[51] (a) M. Rahimi, R. Ghiasi, Solvent effect on isomerization reaction of [(η5-C5H5)(CO)2Re=C(C2HB10H10)(C6H5)] carbene complex to [(η5-C5H5)(CO)(COC2HB10H10)Re≡CC6H5] carbyne complex: A computational investigation. *J. Mol. Liq.*, 265 (2018) 164-171; (b) M.R.P. Heravi, B. Azizi, E.A. Mahmood, A.G. Ebadi, M.J. Ansari, S. Soleimani-Amiri, Molecular simulation of the paracetamol drug interaction with Pt-decorated BC graphene-like nanosheet. *Mol. Simul.*, 48 (2022) 517-525.

[52] K.-Y. Wong, Z. Nie, M.-S. Wong, Y. Wang, J. Liu, Metal–drug coordination nanoparticles and hydrogels for enhanced delivery. *Adv. Mater.*, 36 (2024) e2404053.

[53] T. Nogrady, D.F. Weaver, *Medicinal chemistry: a molecular and biochemical approach*, Oxford University Press, New York (2005).

[54] *Uses of inorganic chemistry in medicine*, Ed: N.P. Farell, RSC Publishing, Cambridge (1999).

[55] R. Ghiasi, A. Zamani, Substituent effect on the electronic properties and nature of the W≡C bond in trans-Cl(OC)(H3P)3W(≡C-para-C6H4X) (X = H, F, SiH3, CN, NO2, SiMe3, CMe3, NH2, NMe2) complexes: a computational quantum chemistry study. *J. Chin. Chem. Soc.*, 64 (2017) 1340-1346.

[56] A. Khanmohammadi, H. Raissi, F. Mollania, L. Hokmabadi, Molecular structure and bonding character of mono and divalent metal cations (Li+, Na+, K+, Be2+, Mg2+, and Ca2+) with substituted benzene derivatives: AIM, NBO, and NMR analyses. *Struct. Chem.*, 25 (2014) 1327-1342.

[57] A. Khanmohammadi, F. Ravari, The influence of cation-π interactions on the strength and nature of intramolecular O···H hydrogen bond in orthohydroxy benzaldehyde compound. *Phys. Chem. Res.*, 5 (2017) 57-68.

[58] M. Mohammadi, F. Alirezapour, A. Khanmohammadi, DFT calculation of the interplay effects between cation–π and intramolecular hydrogen bond interactions of mesalazine drug with selected transition metal ions (Mn+, Fe2+, Co+, Ni2+, Cu+, Zn2+). *Theor. Chem. Acc.*, 140 (2021) 104.

[59] M. Mohammadi, M. Mahinian, A. Khanmohammadi, Theoretical study of stability and electronic characteristics in various complexes of psoralen as an anticancer drug in gas phase, water and CCl4 solutions. *Chem. Res. Chin. Univ.*, 38 (2022) 1414.

[60] A. Hassanpour, M.R.P. Heravi, A. Khanmohammadi, Electronic sensors for alkali and alkaline earth cations based on Fullerene-C60 and silicon doped on C60 nanocages: a computational study. *J. Mol. Model.*, 28 (2022) 148.

[61] M. Pirgheibi, M. Mohammadi, A. Khanmohammadi, A comparative study of interplay effects between the cation-π and intramolecular hydrogen bond interactions in the various complexes of methyl salicylate with Mn+, Fe2+, Co+, Ni2+, Cu+, and Zn2+ cations. *Struct. Chem.*, 32 (2021) 1529.

[62] M. Mohammadi, A. Khanmohammadi, Molecular structure, QTAIM and bonding character of cation–π interactions of mono- and divalent metal cations (Li+, Na+, K+, Be2+, Mg2+ and Ca2+) with drug of acetaminophen. *Theor. Chem. Acc.*, 138 (2019) 101-109.

[63] F. Alirezapour, A. Khanmohammadi, Theoretical study on the interaction of phenylalaninal with group IA (Li+, Na+, K+) and IIA (Be2+, Mg2+, Ca2+) metal cations. *J. Chin. Chem. Soc.*, 68 (2021) 1002.

[64] F. Alirezapour, A. Khanmohammadi, The effect of cation–π interactions on the stability and electronic properties of anticancer drug Altretamine: a theoretical study. *Acta Crystallogr. Sect. C*, 76 (2020) 982.

[65] E.A. Mahmood, M.R.P. Heravi, A. Khanmohammadi, S. Mohammadi-Aghdam, A.G. Ebadi, S. Habibzadeh, DFT calculations, structural analysis, solvent effects, and non-covalent interaction study on the para-aminosalicylic acid complex as a tuberculosis drug: AIM, NBO, and NMR analyses. *J. Mol. Model.*, 28 (2022) 297.

[66] M. Koohi, H. Bastami, Adsorption of biologically active indoline-2-one on C20 nanocage in various surroundings: A DFT enquiry. *Pramana*, 97 (2023) 143.

[67] M. Koohi, H. Bastami, Solvent effect on adsorption of benzylidene oxindole to C20 nanocage: A DFT approach. *J. Phys. Org. Chem.*, 36 (2023) e4505.

[68] M. Koohi, H. Bastami, Investigation of Ti–B nanoheterofullerenes evolved from C20 nanocage through DFT. *Chem. Rev. Lett.*, 6 (2023) 223-234.

[69] M. Koohi, H. Bastami, A quest for stable 2, 2, 9, 9-tetrahaloplumbacyclonona-3, 5, 7-trienylidenes at density functional theory. *Struct. Chem.*, 31 (2020) 877-898.

[70] M. Koohi, H. Bastami, Substituted Hammick carbenes: The effects of fused rings and hetero atoms through DFT calculations. *J. Phys. Org. Chem.*, 33 (2020) e4023.

[71] M.J. Frisch, G.W. Trucks, H.B. Schlegel, G.E. Scuseria, M.A. Robb, J.R. Cheeseman, et al., Gaussian 09, Gaussian, Inc., Wallingford, CT, USA (2009).

[72] J.D. Chai, M. Head-Gordon, Long-range corrected hybrid density functionals with damped atom–atom dispersion corrections. *Phys. Chem. Chem. Phys.*, 10 (2008) 6615.

[73] R. Krishnam, J.S. Binkley, R. Seeger, J.A. Pople, Self-consistent molecular orbital methods 25. Supplementary functions for Gaussian basis sets. *J. Chem. Phys.*, 80 (1984) 3265.

[74] H. Iikura, T. Tsuneda, T. Yanai, K. Hirao, A long-range correction scheme for generalized-gradient-approximation exchange functionals. *J. Chem. Phys.*, 115 (2001) 3540.
[75] J. D. Chai, M. Head-Gordon, Systematic optimization of long-range corrected hybrid density functionals. *J. Chem. Phys.*, 128 (2008) 084106.
[76] https://sites.google.com/site/orcainputlibrary/geometry-optimizations
[77] https://www.cup.uni-muenchen.de/ch/compchem/geom/basic.html
[78] S.B. Boys, F. Bernardi, The calculation of small molecular interactions by the differences of separate total energies. Some procedures with reduced errors. *Mol. Phys.*, 19 (1970) 553.
[79] S. Miertus, E. Scrocco, J. Tomasi, Electrostatic interaction of a solute with a continuum: a direct utilization of AB initio molecular potentials for the prevision of solvent effects. *Chem. Phys.*, 55 (1981) 117–129.
[80] R.F.W. Bader, *Atoms in molecules: A quantum theory*, Oxford University Press, New York (1990).
[81] A.E. Reed, L.A. Curtiss, F. Weinhold, Intermolecular interactions from a natural bond orbital, donor–acceptor viewpoint. *Chem. Rev.*, 88 (1988) 899.
[82] K.F. Biegler, J. Schonbohm, D. Bayles, AIM 2000: a program to analyze and visualize atoms in molecules. *J. Comput. Chem.*, 22 (2001) 545.
[83] T.M. Krygowski, M.K. Cyranski, Separation of the energetic and geometric contributions to the aromaticity of π-electron carbocyclics. *Tetrahedron*, 52 (1996) 1713–1722.
[84] E. Matito, M. Duran, M. Sola', The aromatic fluctuation index (FLU): a new aromaticity index based on electron delocalization. *J. Chem. Phys.*, 122 (2005) 014109–014117.
[85] T. Lu, F. Chen, Multiwfn: a multifunctional wavefunction analyzer. *J. Comput. Chem.*, 33 (2012) 580-592.
[86] P. Pulay, J.F. Hinton, K. Wolinski, In: J.A. Tossel (ed) *Nuclear magnetic shieldings and molecular structure*, vol 386. Kluwer, Dordrecht (1993).
[87] R.F.W. Bader, T.S. Slee, D. Cremer, E. Kraka, Description of conjugation and hyperconjugation in terms of electron distributions. *J. Am. Chem. Soc.*, 105 (1983) 5061–5068.
[88] A. Rahmanzadeh, M. Rezvani, M.D. Ganji, M.T. Moghim, Corrosion protection performance of Laurhydrazide N′-propan-3-one (LHP) adsorbed on zinc surface: A DFT-MD simulation investigation. *Mater. Today Commun.*, 36 (2023) 106946.
[89] R.D. Parra, J. Ohlssen, Cooperativity in intramolecular bifurcated hydrogen bonds: an ab initio study. *J. Phys. Chem. A*, 112 (2008) 3492–3498.
[90] R. Ghiasi, The mono- and di-silanaphthalene: structure, properties, and aromaticity. *J. Mol. Struct. THEOCHEM*, 718 (2005) 225-233.
[91] L. Hokmabady, H. Raissi, A. Khanmohammadi, Interactions of the 5-fluorouracil anticancer drug with DNA pyrimidine bases: a detailed computational approach. *Struct. Chem.*, 27 (2016) 487–504.
[92] C. Garau, A. Frontera, D. Quiñonero, P. Ballester, A. Costa, P.M. Deyà, Cation-π versus anion-π interactions: energetic, charge transfer, and aromatic aspects. *J. Phys. Chem. A*, 108 (2004) 9423–9427.
[93] P.K. Chattaraj, A. Poddar, Molecular reactivity in the ground and excited electronic states through density dependent local and global reactivity parameters. *J. Phys. Chem. A*, 103 (1999) 8691.
[94] R.G. Pearson, Chemical hardness-applications from molecules to solids, VCH-Wiley, Weinheim (1997).
[95] R.G. Parr, L.V. Szentpály, S. Liu, Electrophilicity index. *J. Am. Chem. Soc.*, 121 (1999) 1922.
[96] K.D. Sen, C.K. Jorgensen, *Electronegativity, Structure and Bonding*, Springer Verlag, New York (1987).
[97] R. Ghiasi, M.Z. Fashami, Tautomeric transformations and reactivity of isoindole and sila-indole: A computational study. *J. Theor. Comput. Chem.*, 13 (2014) 1450041.
[98] N. Mohan, C.H. Suresh, A molecular electrostatic potential analysis of hydrogen, halogen, and dihydrogen bonds. *J. Phys. Chem. A*, 118 (2014) 1697.
[99] M. Koohi, H. Bastami, Structure, stability, MEP, NICS, reactivity, and NBO of Si–Ge nanocages evolved from C20 fullerene at DFT. *Monatsh. Chem.*, 151 (2020) 693-710.
[100] N.N. Milani, R. Ghiasi, A. Forghaniha, The impact of solvent polarity on the stability, electronic properties, and 1H NMR chemical shift of the conformers of 2-chloro-3-methylcyclohexan-1-one oxime: a conceptual DFT approach. *J. Appl. Spectrosc.*, 86 (2020) 1123–1131.
[101] M. Rezazadeh, R. Ghiasi, S. Jamehbozorgi, Influence of solvent and electric field on the structure and IR, 31P NMR spectroscopic properties of a titanocene–benzyne complex. *J. Appl. Spectrosc.*, 85 (2018) 526–534.
[102] N. Sadeghi, R. Ghiasi, R. Fazaeli, S. Jamehbozorgi, Quantum chemical study of the solvent effect on the anticancer active molecule of Iproplatin: structural, electronic, and spectroscopic properties (IR, 1H NMR, UV). *J. Appl. Spectrosc.*, 83 (2017) 909–916.